

Fast Alignment Using Rotation Vector and Adaptive Kalman Filter

Hyo-Sung Ahn and Chang-Hee Won[†]

**Department of Electrical Engineering, University of North Dakota
Electrical and Computer Engineering Department, Temple University**

Abstract

A fast and convenient alignment method is proposed in this paper. To improve the speed of convergence, we used rotation vectors instead of traditional Euler angles. Furthermore, we developed an algorithm to automatically tune the measurement noise covariance matrix using adaptive Kalman filtering. Finally, the developed algorithms were applied to an aerial imaging system to automatically geo-locate the centers of the images.

Index Terms – Rotation vector, Alignment, Adaptive Kalman Filter, Aerial Imaging System

[†] Correspondent author, 1947 N. 12th Street, Philadelphia, PA 19122 USA,
Voice: 215-204-7597, Fax: 215-204-5960, E-mail: changheewon@yahoo.com

I. Introduction

This paper uses the rotation vector for the fine alignment dynamics of the inertial navigation system (INS), which is composed of the inertial measurement unit (IMU), inertial navigation equation mechanization, and alignment algorithm. Generally, the accuracy of the initial alignment depends on the IMU's performance. In the case of a relatively low-cost tactical grade IMU, tilt angles can be estimated accurately from the leveling procedure using accelerometer outputs. However, it takes a long time to estimate the azimuth angle in the gyro-compassing procedure [1-3]. Moreover, the filter convergence characteristic is related to the coupling between the estimated states and the reference measurements. Thus, our main interest will be in increasing the coupling between the reference measurements and the estimated states. In this research, the rotation vector was used to increase the coupling between the measurements and estimated states, and consequently improve the filter convergence speed.

The rotation vector has been studied by several researchers [19-23]. Rotation vector transforms the (x, y, z) coordinate system to the (x', y', z') coordinate system by rotating about a vector, $\underline{\rho} = [\rho_x \quad \rho_y \quad \rho_z]^T$, in the amount specified by the magnitude of $|\underline{\rho}|$, as shown in Figure 1. The right hand rule decides the positive rotation direction. Because the rotation vector expresses the kinematics of the body coordinate frame, the rotation vector can be used instead of the Euler angles to express the attitude transformation.

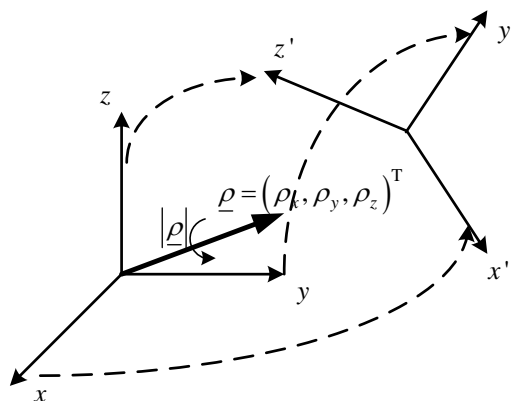


Figure 1. Rotation vector.

After Bortz [19] derived the relationship between the rotation vector and directional cosine matrix (DCM) in 1971, a number of other researchers derived similar kinematic equations using various different approaches [20, 22]. It has been known that the rotation vector can be used to improve the attitude accuracy of the navigation system [21]. Recently, the rotation vector was used for the tightly coupled GPS/INS integration, but not for the alignment [18]. The references [19-22] focus on the theoretical derivation and references [18, 23] show the practical application.

In a typical alignment method, Euler angles are used to integrate the attitude transformation matrix of the body frame with respect to a reference frame [1-6, 8-14]. In the Euler angle based method, the measurement sensitivity matrix depends on the observer's latitude, and the fixed earth rotation rates limit the coupling amount. However, in the new method, because there is a tight coupling between the estimated states and the reference measurements, the azimuth angle is estimated much faster than the Euler angle based method.

Note that the measurement sensitivity matrix does not depend on the observer's latitude because the rotation vector based method estimates the gyroscope output directly and this output is used as the measurements.

Here, a comment is in order for another alignment method, which uses quaternions for the initial attitude estimation. Quaternion formulations are commonly used in INS mechanizations, but not in attitude error representations. Moreover, as noted in reference [4, p. 87], quaternion based alignment algorithm requires more time than the Euler angle based alignment method. Thus, we do not compare this method with the rotation vector based method.

Another important issue in the alignment is tuning the measurement noise covariance matrix. It is difficult to manually tune the measurement noise density with the time varying noises such as the navigation frame disturbance. Thus, in this paper, we propose to use the adaptive Kalman filtering method to automatically estimate the measurement noise covariance matrix. To automatically tune both process and measurement noise covariance matrices, we needed the relationship between the process noise and measurement noise, but determining this relationship was difficult for our system. So the process noise was tuned manually.

The adaptive Kalman filter has been available for more than three decades since Magil designed weighting functions for the conditional estimates in 1965 [24]. After

Magil's work, various researchers have designed multiple model adaptive estimators (MMAE). The MMAE is composed of a bank of Kalman filters [25]. The bank of Kalman filters has the elemental Kalman filters for each system model. So, MMAE is a costly algorithm to implement in terms of amount of computation time [25-27]. Another use of adaptive Kalman filter is in the self-tuning estimation algorithm. Maybeck investigated this class of algorithm in his book [38].

In real world applications, many researchers have used adaptive Kalman filter for the stochastic dynamic systems [4, 28-37]. Their applications vary from the image processing to the satellite navigation. In the navigation applications, Wang and Dai used the adaptive Kalman filter method to resolve the GPS dual phase ambiguity [30-31]. Wira and Urban designed the 3-dimensional visual servo systems using adaptive Kalman filter [32-33]. Dakshayani and Ananthasayanam designed the adaptive Kalman filter for the satellite orbit determination using fading memory method [34]. Sasiadek and Wang designed the fuzzy logic adaptive controller (FLAC) to prevent the Kalman filter from diverging [37]. Here, we use the adaptive estimation method introduced in [38], and apply it to the IMU alignment problem.

The University of North Dakota is working on the Airborne Environmental Research Observational Camera (AEROCam) project, which takes multi-spectral digital images of the fields for precision farming. As a part of the project, we are using DGPS/INS integration to

automatically determine the geo-location of the aerial image centers. Fast and convenient alignment algorithm development is a part of this DGPS/INS integration. Consequently, we will apply our algorithm to the AEROCam system and perform alignment using the rotation vector and adaptive Kalman filter.

This paper is organized as follows. The nonlinear dynamic model using rotation vector for the alignment is presented in Section II. The measurement dynamics based on the Euler angles is briefly reviewed in Section III. In Section IV, the adaptive Kalman filter for the initial alignment is designed. In Section V, the simulations are performed to verify the superiority of the rotation vector method and in Section VI, we will show the field test results. The conclusions are given in Section VII.

II. New State Dynamic Model for Alignment

In this section, the nonlinear state dynamic model using the rotation vector is presented for the fine alignment algorithm of INS. In the rotation vector based alignment dynamics, the gyroscope outputs are directly measured and estimated due to the feedback structure of the rotation vector. The feedback structure means that the gyroscope output in the body frame is approximated from the previous rotation vector. This characteristic gives the tight coupling between the estimated attitude errors and reference measurements. Due to this coupling, the heading angle is estimated much faster than the Euler angle based alignment

method. The zero velocity information of the IMU on the navigation coordinate frame is used for the reference measurement. Thus, velocity and rotation vector components are used as system states in the nonlinear dynamics model, while the position and sensor noises are ignored. The velocity and rotation vector are also used as the measurements. Here, we use the numerical Jacobian method.

This section is organized as follows. The nonlinear system dynamic models are given in Eq. (1) and Eq. (6) for velocity and angle predictions. The nonlinear measurement dynamics are given in Eq. (8) and Eq. (9) for velocity and angular rate models, respectively.

A. Velocity Dynamics Model

References [5, p. 199] express velocity dynamics in the North-East-Down (NED) coordinate frame. By transforming into East-North-Up (ENU) coordinate frame, the velocity dynamics are expressed as

$$\begin{bmatrix} \dot{v}_E \\ \dot{v}_N \\ \dot{v}_U \end{bmatrix} = \begin{bmatrix} f_E + \left(\frac{v_E}{(R_\Phi + h) \cos(\lambda)} + 2\omega_{ie} \right) v_N \sin(\lambda) - \frac{v_E v_U}{R_\Phi + h} - 2\omega_{ie} v_U \cos(\lambda) \\ f_N - \left(\frac{v_E}{(R_\Phi + h) \cos(\lambda)} + 2\omega_{ie} \right) v_E \sin(\lambda) - \frac{v_N v_U}{R_\lambda + h} \\ f_U + \frac{v_E^2}{R_\Phi + h} + \frac{v_N^2}{R_\lambda + h} + v_E 2\omega_{ie} \cos(\lambda) \end{bmatrix} - \underline{g} + \underline{w}_1, \quad (1)$$

where \underline{g} is the earth gravity force including the gravity anomaly components, h is the altitude, R_Φ is the earth transverse radius, and R_λ is the earth meridional radius. λ is the known initial latitude of the IMU, and ω_{ie} is the earth rotation rate. (v_E, v_N, v_U) is the velocity in the ENU coordinate frame. The velocity dynamic model noise \underline{w}_1 , which is

assumed as Gaussian white noise, includes the earth radius model error, gravity anomaly model error, initial position error, and uncompensated constant bias noises. The acceleration in the ENU coordinate frame, \underline{f}^n , is calculated by

$$\underline{f}^n \equiv \begin{bmatrix} f_E \\ f_N \\ f_U \end{bmatrix} = C_b^e A^a \left[\underline{f}^b - \underline{b}^a \right], \quad (2)$$

where C_b^e is the attitude transformation matrix from the body frame to the ENU coordinate frame, \underline{f}^b is the accelerometer output in the body frame, and \underline{b}^a is the accelerometer bias noise. The scale factor ($SF_{ii}^a |_{i=1,2,3}$) and misalignment ($MA_{jk}^a |_{j,k=1,2,3, \text{ and } j \neq k}$) matrix of the accelerometers is expressed by

$$A^a = \begin{bmatrix} I_{3 \times 3} & \begin{bmatrix} SF_{11}^a & MA_{12}^a & MA_{13}^a \\ MA_{21}^a & SF_{22}^a & MA_{23}^a \\ MA_{31}^a & MA_{32}^a & SF_{33}^a \end{bmatrix} \end{bmatrix}.$$

The scale factor and misalignment values are given from the IMU specification. Notice that the bias noise, \underline{b}^a , is composed of three different noise components, which are constant bias, turn-on bias and random walk noise. The constant bias noise is given from the data sheet.

But the turn-on bias has to be calibrated, and the random walk noise has to be estimated.

The turn-on bias is calibrated every time IMU is turned on. In this paper, the accelerometer on the Z-axis is calibrated based on the tilt angle from the coarse alignment. This will be shown in Section VI. We ignore the random walk noise because the random walk noise is relatively small when we estimate the attitude errors relatively fast using the rotation vector.

The rotation vector with respect to the ENU coordinate frame is related to the attitude

transformation matrix of Eq. (2) from [18, p. 348] by

$$C_b^e = \left(\cos(|\underline{\rho}|) \mathbf{I}_{3 \times 3} + \frac{1 - \cos(|\underline{\rho}|)}{|\underline{\rho}|^2} \underline{\rho} \cdot \underline{\rho}^T + \frac{\sin(|\underline{\rho}|)}{|\underline{\rho}|} [\underline{\rho} \otimes] \right), \quad (3)$$

where the rotation vector is $\underline{\rho} \equiv [\rho_E \quad \rho_N \quad \rho_U]^T$ and the skew symmetric matrix of the

rotation vector is $[\underline{\rho} \otimes] = \begin{bmatrix} 0 & -\rho_U & \rho_N \\ \rho_U & 0 & -\rho_E \\ -\rho_N & \rho_E & 0 \end{bmatrix}$. The magnitude of the rotation vector is

calculated from

$$|\underline{\rho}| = (\underline{\rho}^T \cdot \underline{\rho})^{1/2}. \quad (4)$$

B. Attitude Dynamics Model

Various forms for the attitude kinematics of the rotation vector have been introduced in the literature [18-23]. One of these forms is given by

$$\dot{\underline{\rho}} = \left\{ \mathbf{I}_{3 \times 3} + \frac{1}{2} [\underline{\rho} \otimes] + \frac{1}{\underline{\rho}^T \cdot \underline{\rho}} \left(1 - \frac{\underline{\rho} \cdot \sin|\underline{\rho}|}{2(1 - \cos|\underline{\rho}|)} \right) [\underline{\rho} \otimes]^2 \right\} \underline{\omega}^b, \quad (5)$$

where $\underline{\omega}^b$ is the angular rate in the body frame. However, this form does not include the

earth rotation rate, and velocity related angular rates. When the earth rotation rate, Coriolis

force effect, and centrifugal acceleration are considered, the kinematics equation, Eq. (5), of

the rotation vector can be expressed in an alternative forms, which is somewhat nonstandard,

as [18, p. 356]:

$$\underline{\dot{\rho}} = \frac{\partial \dot{\rho}}{\partial \underline{\omega}^b} \underline{\omega}^b + \frac{\partial \dot{\rho}}{\partial \underline{\omega}^e} \underline{\omega}^e + \underline{w}_2 \quad (6)$$

where

$$\frac{\partial \dot{\rho}}{\partial \underline{\omega}^b} = \underline{1}_\rho \cdot \underline{1}_\rho^T + \frac{|\underline{\rho}| \sin|\underline{\rho}|}{2[1 - \cos|\underline{\rho}|]} \left[\mathbf{I}_{3 \times 3} - \underline{1}_\rho \cdot \underline{1}_\rho^T \right] + \frac{|\underline{\rho}|}{2} \left[\underline{1}_\rho \otimes \right],$$

$$\frac{\partial \dot{\rho}}{\partial \underline{\omega}^e} = -\underline{1}_\rho \cdot \underline{1}_\rho^T - \frac{|\underline{\rho}| \sin|\underline{\rho}|}{2[1 - \cos|\underline{\rho}|]} \left[\mathbf{I}_{3 \times 3} - \underline{1}_\rho \cdot \underline{1}_\rho^T \right] + \frac{|\underline{\rho}|}{2} \left[\underline{1}_\rho \otimes \right],$$

and $\underline{1}_\rho = \frac{\underline{\rho}}{|\underline{\rho}|}$. The dynamics model error \underline{w}_2 , which is also assumed as Gaussian white

noise, includes the earth radius model error and uncompensated gyroscope noises. The

transformed rotation rate ($\underline{\omega}^e$) from the IMU body frame to the ENU coordinate frame

includes earth rotation rate ($\underline{\omega}_e^{enu}$), centrifugal acceleration ($\underline{\omega}^a$) and Coriolis effect ($\underline{\omega}^c$).

Using [18, p. 260] for $\underline{\omega}_e^{enu}$ and $\underline{\omega}^c$ with $\underline{\omega}^a = \begin{bmatrix} 0 & 0 & \frac{v_E \tan(\lambda)}{R_\Phi + h} \end{bmatrix}^T$, we obtain

$$\underline{\omega}^e = \underline{\omega}_e^{enu} + \underline{\omega}^a + \underline{\omega}^c = \begin{bmatrix} 0 \\ \omega_{ie} \cos(\lambda) \\ \omega_{ie} \sin(\lambda) \end{bmatrix} + \begin{bmatrix} 0 \\ 0 \\ \frac{v_E \tan(\lambda)}{R_\Phi + h} \end{bmatrix} + \begin{bmatrix} -\frac{v_N}{R_\lambda + h} \\ \frac{v_E}{R_\Phi + h} \\ 0 \end{bmatrix}. \quad (7)$$

Compensating the gyroscope bias noises (\underline{b}^g), gyroscope scale factor ($SF_{ii}^g |_{i=1,2,3}$) and

gyroscope misalignment ($MA_{jk}^g |_{j,k=1,2,3, \text{ and } j \neq k}$), the angular rate in the body frame is

expressed as

$$\underline{\omega}^b = A^g \left(\underline{\omega}^e - \underline{b}^g \right), \text{ and}$$

$$A^g = \left[\mathbf{I}_{3 \times 3} - \mathbf{M}^g \right] = \left[\mathbf{I}_{3 \times 3} - \begin{bmatrix} SF_{11}^g & MA_{12}^g & MA_{13}^g \\ MA_{21}^g & SF_{22}^g & MA_{23}^g \\ MA_{31}^g & MA_{32}^g & SF_{33}^g \end{bmatrix} \right].$$

The scale factor, the misalignment, and the constant bias noise are given from the gyroscope specification data. However, the turn-on bias noise should be calibrated every time

gyroscope is turned on. The gyroscopes are calibrated based on DGPS heading angle.

Thus, the bias noise, \underline{b}^g , is estimated as the sum of the constant bias and estimated turn-on bias noise. Random walk noise is ignored. Section VI explains this calibration method.

C. Measurement Model

The velocity and angular rate are used as reference measurements. The measurement model for the velocity is easily designed as

$$\begin{bmatrix} \tilde{v}_E \\ \tilde{v}_N \\ \tilde{v}_U \end{bmatrix} = \begin{bmatrix} 1 & 0 & 0 \\ 0 & 1 & 0 \\ 0 & 0 & 1 \end{bmatrix} \begin{bmatrix} v_E \\ v_N \\ v_U \end{bmatrix} + \underline{v}_1, \quad (8)$$

where measurement model error \underline{v}_1 represents the Gaussian white noise of the

accelerometer output. The real measurements of the velocity are all zero because the IMU

is in the stationary state. The measurement dynamic model for the rotation rate in the body

frame is derived from Eq. (6). This is given from [18, p. 261] as

$$\underline{\tilde{\omega}}^b = \left(\frac{\partial \underline{\dot{\rho}}}{\partial \underline{\omega}^b} \right)^{-1} \left[\underline{\dot{\rho}} - \frac{\partial \underline{\dot{\rho}}}{\partial \underline{\omega}^e} \begin{bmatrix} -\frac{v_N}{R_\lambda + h} \\ \frac{v_E}{R_\Phi + h} + \omega_{ie} \cos(\lambda) \\ \omega_{ie} \sin(\lambda) + \frac{v_E \tan(\lambda)}{R_\Phi + h} \end{bmatrix} \right] + \underline{v}_2, \quad (9)$$

where \underline{v}_2 represents the gyroscope measurement white noises. In reference [18], the derivative of the rotation vector with respect to the time, $\underline{\dot{\rho}}$, in Eq. (9) is estimated as system states by differentiating Eq. (6) one more time. In Eqs. (7) and (9), the earth rotation rate, Coriolis effect, and the earth centrifugal acceleration have been compensated, thus $\underline{\dot{\rho}}$ corresponds to the rotation of the IMU in the body frame. For the stationary case, $\underline{\dot{\rho}}$ is assumed to be zero for the alignment purposes.

III. Euler Angle Based Measurement Model

In this section, we review the traditional alignment method based on the Euler angles to compare it with our method. The state dynamics are well established; see [1-5, 8-14, 39] for example. On the other hand, the measurement model is system dependent and it is not as well established as the state dynamic model. Thus, we will present the derivation of the measurement model for the Euler angle-based alignment in this section.

Accelerometer measurements and gyroscope measurement are used for the measurement residuals of Kalman filter. The error of the calculated acceleration, $\delta \underline{f}^n$, in the navigation frame is

$$\delta \underline{f}^n = - \begin{bmatrix} 0 & -\varepsilon_D & \varepsilon_E \\ \varepsilon_D & 0 & -\varepsilon_N \\ -\varepsilon_E & \varepsilon_N & 0 \end{bmatrix} \begin{bmatrix} 0 \\ 0 \\ g \end{bmatrix} + C_b^n \delta \underline{f}^b + \underline{f}_d, \quad (10)$$

where C_b^n is the coordinate transformation from the body frame to the NED frame; $\delta \underline{f}^b$ is accelerometer measurement uncertainties; and \underline{f}_d is the navigation frame disturbance noise.

The skew symmetric matrix of $(\varepsilon_N, \varepsilon_E, \varepsilon_D)$ represents the error of the attitude transformation matrix.

The error of the calculated angular rate in the navigation frame is

$$\delta \underline{\omega}^n = \underline{\omega}_e^{ned} - \underline{\omega}^n \quad (11)$$

$$= \begin{bmatrix} 0 & -\varepsilon_D & \varepsilon_E \\ \varepsilon_D & 0 & -\varepsilon_N \\ -\varepsilon_E & \varepsilon_N & 0 \end{bmatrix} \begin{bmatrix} \omega_N \\ \omega_E \\ \omega_D \end{bmatrix} + C_b^n \delta \underline{\omega}^b + \underline{w}_d \quad (12)$$

where $\delta \underline{\omega}^b$ is gyro measurement uncertainties; $\underline{\omega}^n$ is gyro measurement in NED frame;

$\underline{\omega}_e^{ned} = [\omega_N \ \omega_E \ \omega_D]^T$ is earth rotation rate in NED frame; and \underline{w}_d is the navigation frame disturbance noise.

Note that the sensor measurement uncertainties ($\delta \underline{f}^b$ and $\delta \underline{\omega}^b$) and disturbance errors (\underline{f}_d and \underline{w}_d) are estimated by an adaptive Kalman filter as explained in

Section IV. In the Euler angle based method, the system state vector consists of velocity

errors $\delta \underline{v}^n = [\delta v_N \ \delta v_E \ \delta v_D]^T$ in the navigation frame and attitude errors

$\underline{\varepsilon} = [\varepsilon_N \ \varepsilon_E \ \varepsilon_D]^T$. The measurement model is given as

$$\begin{bmatrix} \delta\tilde{v}_N \\ \delta\tilde{v}_E \\ \delta\tilde{\omega}_N \\ \delta\tilde{\omega}_E \\ \delta\tilde{\omega}_D \end{bmatrix} = \begin{bmatrix} 1 & 0 & 0 & 0 & 0 \\ 0 & 1 & 0 & 0 & 0 \\ 0 & 0 & 0 & \omega_D & 0 \\ 0 & 0 & -\omega_D & 0 & \omega_N \\ 0 & 0 & 0 & \omega_N & 0 \end{bmatrix} \begin{bmatrix} \delta v_N \\ \delta v_E \\ \varepsilon_N \\ \varepsilon_E \\ \varepsilon_D \end{bmatrix} + \underline{v}, \quad (13)$$

where \underline{v} is the measurement model error vector, and it is assumed as Gaussian white noise.

The actual measurements are accelerometer outputs, gyroscope outputs, zero velocity, and earth rotation rates with respect to the NED frame.

For the adaptive Kalman filter, we find the actual velocity error measurement of Eq.

(10) by calculating the velocity error on the NED frame from the actual measurements.

First we estimate the IMU velocity, $\underline{v}^n = [v_N \ v_E \ v_D]^T$, on the NED frame as

$$(\underline{v}^n)_k = (\underline{v}^n)_{k-1} + \Delta t \times \left(C_b^n \right)_k \left(\underline{f}^b \right)_k, \quad (14)$$

where \underline{f}^b is the accelerometer output in the body frame, and the discrete time notation, k , is used because IMU outputs the data with Δt interval. Because the down direction is not considered in Eq. (13), we do not have to consider the gravity force. Eq. (14) shows that the current velocity depends on the previous velocity and current acceleration. Then we can determine the measured velocity error as

$$(\delta\tilde{v}^n)_k = \underline{0} - (\underline{v}^n)_k = -(\underline{v}^n)_k, \quad (15)$$

where $\underline{0}$ is the zero velocity vector in the navigation frame and $(\underline{v}^n)_k$ is from Eq. (14).

Next, the measured angular rate errors, $\delta\tilde{\omega}^n = [\delta\tilde{\omega}_N \ \delta\tilde{\omega}_E \ \delta\tilde{\omega}_D]^T$, in the NED frame are derived from Eq. (12) as

$$\left(\delta\tilde{\underline{\omega}}^n\right)_k = \underline{\omega}_e^{ned} - \left(C_b^n\right)_k \left(\underline{\omega}^b\right)_k, \quad (16)$$

where $\underline{\omega}^b$ is the gyroscope output in the body frame. Finally, $\left(\delta\tilde{\underline{v}}^n\right)_k$ and $\left(\delta\tilde{\underline{\omega}}^n\right)_k$ are used as actual measurements in the Kalman filter.

IV. Adaptive Kalman Filter Design

It is expected that the navigation frame disturbances have high frequency noises, and their amplitude and spectral density may be time varying and not known accurately [4-5]. Thus, it is difficult to find the accurate noise density without the precise knowledge of the model and noise characteristics. Therefore, we have applied the adaptive Kalman filtering method to tune the measurement noise covariance automatically.

For the rotation vector-based alignment, the discrete linearized Kalman filter equations are used. The overall design procedures of the linearized Kalman filter are given in [6, p. 169]. The nonlinear nominal trajectory model is given as

$$x_k^{\text{NOM}} = f\left(x_{k-1}^{\text{NOM}}, k-1\right),$$

where $\{x_{k-1}^{\text{NOM}}\}$ is the sequence referring to the nominal trajectory obtained when the random variates assume their expected values [6, p. 162]. In our system, Eqs. (1) and (6) are the nonlinear system dynamic models. The nonlinear measurement models, $z_k = h(x_k, k) + v_k$, are given in Eqs. (8) and (9). Note that even though Eqs. (1), (6), (8), and (9) are in continuous time, for the computer simulations, they are calculated in discrete dynamics. To

implement the adaptive Kalman filter algorithm in the simulations, we change the continuous time Eqs. (1), (6), (8), and (9) to discrete time. The linear perturbation, which is defined as $\delta x \equiv x - x^{\text{NOM}}$, is estimated as state in the Kalman filter. If the estimated perturbation is denoted as $\delta \hat{x}$, then the prediction of the linear perturbation is given as

$$\delta \hat{x}_k(-) = \Phi_{k-1} \delta \hat{x}_{k-1}(+),$$

where $\hat{x}_k(-)$ is the *a priori* estimate of x_k and $\hat{x}_{k-1}(+)$ is the *a posteriori* value of the previous estimate. The state prediction matrix, Φ_{k-1} , is calculated from the first order approximation by

$$\Phi_{k-1} \approx \left. \frac{\partial f(x, k-1)}{\partial x} \right|_{x=x_{k-1}^{\text{NOM}}}.$$

In the linearized Kalman filter for the rotation vector-based alignment, the actual measurements are zero velocity from Eq. (8) and the gyroscope output in the body frame from Eq. (9). If the actual measurements are denoted by $\tilde{z}_k = \begin{bmatrix} \delta \tilde{v}^n & \delta \tilde{\omega}^n \end{bmatrix}^T$, the measurement residuals, r_k , are defined as

$$r_k = h_k(x_k^{\text{NOM}}) - \tilde{z}_k - H_k \delta \hat{x}_k(-), \quad (17)$$

where the measurement sensitivity matrix is approximated by $H_k \approx \left. \frac{\partial h(x, k)}{\partial x} \right|_{x=x_k^{\text{NOM}}}$. Now,

by using Eq. (17) and the computed *a priori* covariance matrix [6, p.169]

$$P_k(-) = \Phi_{k-1} P_{k-1}(+) \Phi_{k-1}^T + Q_{k-1},$$

where Q_{k-1} is the process noise covariance and $P_{k-1}(+)$ is a *posteriori* covariance matrix,

then the measurement noise covariance is estimated from [38, p. 122] as

$$R_k = \frac{1}{N} \sum_{i=k-N+1}^k \left\{ r_i r_i^T - H_i P_i(-) H_i^T \right\}, \quad (18)$$

where N is the number of samples.

A better conditioned estimate is given in [38, p. 123] for Eq. (18) as

$$R_k = \frac{1}{N} \sum_{i=k-N+1}^k \left\{ \left[h_i(x_i^{\text{NOM}}) - \tilde{z}_i - H_i \delta \hat{x}_i(+), \right. \right. \\ \left. \left. + H_i P_i(+), H_i^T \right] \left[h_i(x_i^{\text{NOM}}) - \tilde{z}_i - H_i \delta \hat{x}_i(+), \right. \right. \\ \left. \left. + H_i P_i(+), H_i^T \right]^T \right\}. \quad (19)$$

However, as pointed out in [38, p. 123], $H_k \delta \hat{x}_k(+)$ and $P_k(+)$ are not calculated in the estimation algorithm. Thus, we estimate $\delta \hat{x}_k(+)$ and $P_k(+)$ with the known closest values which are the previous step values, $\delta \hat{x}_{k-1}(+)$ and $P_{k-1}(+)$, in Eq. (19).

Consequently, we obtain

$$R_k = \frac{1}{N} \sum_{i=k-N+1}^k \left\{ \left[h_i(x_i^{\text{NOM}}) - \tilde{z}_i - H_i \delta \hat{x}_{i-1}(+), \right. \right. \\ \left. \left. + H_i P_{i-1}(+), H_i^T \right] \left[h_i(x_i^{\text{NOM}}) - \tilde{z}_i - H_i \delta \hat{x}_{i-1}(+), \right. \right. \\ \left. \left. + H_i P_{i-1}(+), H_i^T \right]^T \right\}. \quad (20)$$

Now, we compare the relative coupling in the measurement sensitivity matrices between the rotation vector-based method and the Euler angle-based method. From Eq. (13), the attitude components of the measurement sensitivity matrix of the Euler angle-based alignment method are

$$H^{\text{Euler}} = \begin{bmatrix} 0 & \omega_D & 0 \\ -\omega_D & 0 & \omega_N \\ 0 & \omega_N & 0 \end{bmatrix}. \quad (21)$$

So, when the alignment is performed at the latitude of 47.9 degrees, the earth rotation rates

are calculated as $\omega_D = 7.29 \times 10^{-5} \times \sin(47.9^\circ) = 5.41 \times 10^{-5}$ (rad/s), and

$\omega_N = 7.29 \times 10^{-5} \times \cos(47.9^\circ) = 4.89 \times 10^{-5}$ (rad/s), respectively. After the Kalman filter

converged, in our method the attitude components of the measurement sensitivity matrix are

numerically calculated from Eq. (9) as

$$\mathbf{H}^{Rotation} = \begin{bmatrix} 6.79 \times 10^{-6} \text{ (rad/s)} & 2.69 \times 10^{-5} \text{ (rad/s)} & 3.3 \times 10^{-5} \text{ (rad/s)} \\ -5.68 \times 10^{-5} \text{ (rad/s)} & 2.06 \times 10^{-6} \text{ (rad/s)} & 9.24 \times 10^{-6} \text{ (rad/s)} \\ 4.02 \times 10^{-5} \text{ (rad/s)} & 1.61 \times 10^{-5} \text{ (rad/s)} & 1.557 \times 10^{-5} \text{ (rad/s)} \end{bmatrix}. \quad (22)$$

Therefore, we know that matrix $\mathbf{H}^{Rotation}$ gives the tighter coupling than matrix \mathbf{H}^{Euler} of Eq.

(21). That is, five elements of \mathbf{H}^{Euler} in Eq. (21) are zeros while all elements of $\mathbf{H}^{Rotation}$

in Eq. (22) have values, which provide tighter cross-coupling between $\underline{\omega}^b$ and $\underline{\rho}$. The

magnitudes of elements of $\mathbf{H}^{Rotation}$ in Eq. (22) are comparable to the magnitudes of ω_D

and ω_N , however in the early stage of Kalman filter the magnitudes of $\mathbf{H}^{Rotation}$ are much

larger than the magnitudes given in Eq. (22). In other words, $\mathbf{H}^{Rotation}$ in Eq. (22)

represents the sensitivity matrix after the Kalman filter converged. Moreover, the

measurement sensitivity matrix of the Euler angle based method depends on the latitude

because the earth rotation rate vector at the measurement position is used. On the contrary,

the measurement sensitivity matrix of the rotation vector based method does not depend on

the latitude. Thus, the measurement sensitivity matrix designed from the rotation vector has

the following two advantages: $\mathbf{H}^{Rotation}$ does not depend on the observer's latitude and

$\mathbf{H}^{Rotation}$ has the tighter coupling than \mathbf{H}^{Euler} .

Figure 2 shows the overall alignment procedure of the rotation vector based method.

The coarse alignment angles in Figure 2 are generated by Euler angles [1, 5]. Thus, the Euler angles of the coarse alignment have to be transformed into rotation vector. When the attitude transformation matrix is given as C_b^e from the coarse alignment, the rotation vector is determined by

$$\rho_E = \frac{|\underline{\rho}|}{\sin|\underline{\rho}|} a_{32}, \quad \rho_N = \frac{|\underline{\rho}|}{\sin|\underline{\rho}|} a_{13}, \quad \rho_U = \frac{|\underline{\rho}|}{\sin|\underline{\rho}|} a_{21}, \quad (23)$$

where

$$A \equiv a_{ij} |_{i,j=1,2,3} = \frac{1}{2} (C_b^e - C_e^b), \text{ and}$$

$$|\underline{\rho}| = \tan^{-1} \left(\frac{\sqrt{a_{32}^2 + a_{13}^2 + a_{21}^2}}{\frac{\text{tr}[C_b^e] - 1}{2}} \right).$$

Note that $C_e^b = (C_b^e)^T$. Attitude and velocity are propagated by 4th order Runge-Kutta method. Zero velocity and gyroscope output are used as the measurements in adaptive Kalman filter. Figure 2 also shows that the attitude and velocity are propagated after the attitude and velocity errors are estimated.

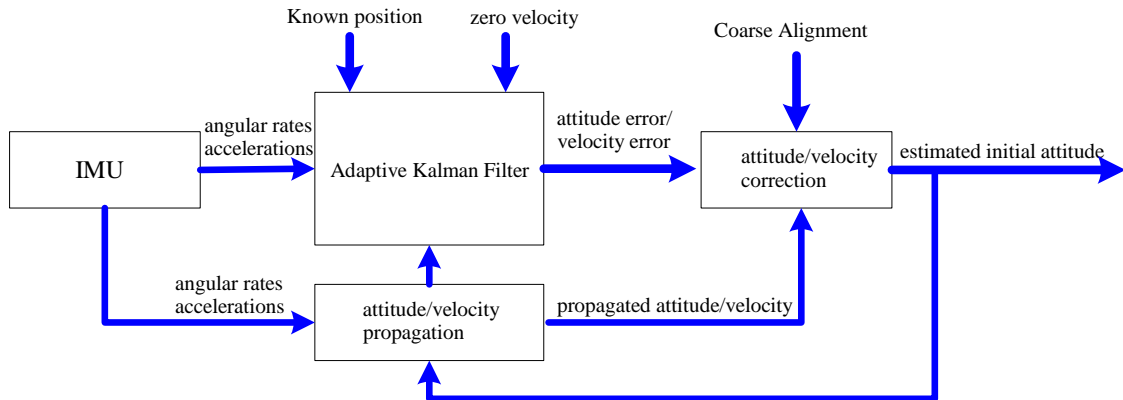


Figure 2. Rotation vector based fine alignment block diagram.

V. Simulations

We developed an IMU model for the simulation purposes. In our IMU model, it was assumed that the constant bias noise components were compensated. Then, the bias noises were modeled by first-order Gauss-Markov process, which used the autocorrelation time constant. The autocorrelation time constant used in the simulation was 7000 seconds, because the autocorrelation time constant of the tactical grade IMU used in the field test was 7000 seconds. The same random walk noise standard deviation values as the IMU specification data sheet were used in the simulation. The following equations show the simulated bias noises of the IMU for accelerometer and gyroscope, respectively.

$$\dot{\underline{b}}^a = -\frac{1}{\tau_a} \underline{b}^a + \sqrt{2\underline{\sigma}_a^2 \underline{\beta}^a} u(t), \text{ and } \dot{\underline{b}}^g = -\frac{1}{\tau_g} \underline{b}^g + \sqrt{2\underline{\sigma}_g^2 \underline{\beta}^g} u(t)$$

where \underline{b}^a and \underline{b}^g are the bias noise vectors of accelerometers and gyroscopes; τ_a and τ_g are the autocorrelation time constants; $\underline{\sigma}_a$ and $\underline{\sigma}_g$ are the random walk noise standard deviations, whose values are given as $\sigma_a = 50 \mu\text{-g}/\sqrt{\text{Hz}}$ and $\sigma_g = 0.02 \text{ deg}/\sqrt{\text{Hz}}$; $\underline{\beta}^a$ and $\underline{\beta}^g$ are the reciprocal time constants; and $u(t)$ is the zero-mean white noise with the covariance of one.

If the true tilt angles are given as the roll angle (ϕ) and the pitch angle (θ), then the accelerometer outputs are modeled as follows:

$$\underline{f}^b = \begin{bmatrix} \sin(\theta) \\ -\cos(\theta)\sin(\phi) \\ -\cos(\theta)\cos(\phi) \end{bmatrix} \underline{g}^n$$

where \underline{g}^n is the gravity force vector in the reference navigation frame. Then, by considering the bias noise and measurement noise, the accelerometer measurements are modeled as

$$\underline{\tilde{f}}^b = \underline{f}^b + \underline{b}^a + \begin{bmatrix} 0.01 \\ 0.01 \\ 0.1 \end{bmatrix} u(t). \quad (24)$$

When the true heading angle (φ) and latitude (λ) are known, the true gyroscope outputs are given as

$$\underline{\omega}^b = \begin{bmatrix} \omega_{ie} \cos \lambda \cos(\varphi) \\ \omega_{ie} \cos \lambda \cos(\varphi + 90^\circ) \\ -\omega_{ie} \sin \lambda \end{bmatrix},$$

where ω_{ie} is the earth rotation rate. Then, the gyroscope measurements are modeled as

$$\underline{\tilde{\omega}}^b = \underline{\omega}^b + \underline{b}^g + \begin{bmatrix} 3.4 \times 10^{-6} \\ 3.6 \times 10^{-6} \\ 5.4 \times 10^{-6} \end{bmatrix} u(t). \quad (25)$$

Initially, 5 degrees of azimuth error and 0.5 degrees of tilt error are assumed. As commented earlier, the measurement noise covariance was estimated automatically from the adaptive Kalman filter. The process noise covariance is given in Table 1, which is also used in the field test. We determined this process noise covariance experimentally.

Table 1. The standard deviation of the process noise.

Position covariance		Attitude covariance	
East velocity (m/s)	2.5×10^{-5}	East rotation vector (radian)	4.4×10^{-8}
North velocity (m/s)	2.5×10^{-5}	North rotation vector (radian)	4.4×10^{-8}
Up velocity (m/s)	3.3×10^{-5}	Up rotation vector (radian)	4.4×10^{-8}

Figure 3 shows the estimated azimuth angles and real azimuth angle. The azimuth angle estimated by the rotation vector method follows the true value more closely than the Euler angle based method. The figure shows that the estimated azimuth angle using Euler angle-based method (dashed line) undershoots about 14 degrees before converging to the true value of -45 degrees. It also shows that the estimated azimuth angle using the rotation vector method (solid line) overshoots about 2 degrees, and it rapidly converges to the true value. In the rotation vector based-method, it takes about 3 seconds to converge to within ± 1 degree of the true value, while in the case of the Euler angle based-method, it takes about 13 seconds to converge within ± 1 degree of the true value.

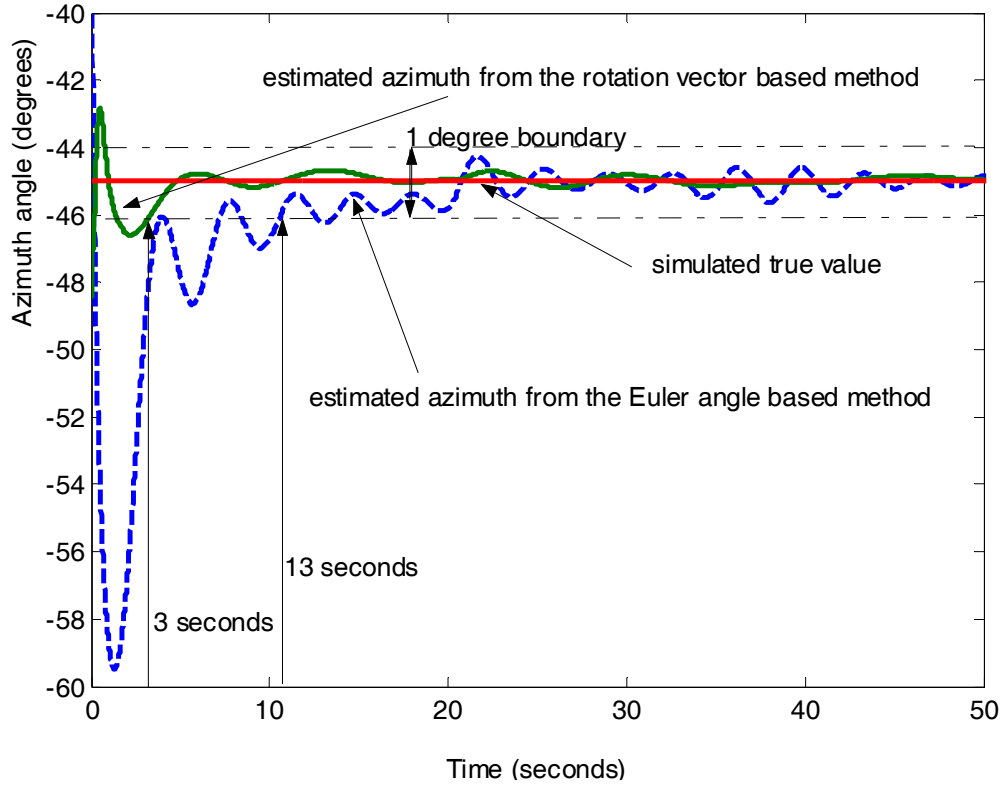


Figure 3. The true reference azimuth angle and estimated azimuth angles.

Figure 4 shows that the estimated measurement noise densities are close to the simulated true values. From Eq. (24), the simulated gyroscope X-axis, Y-axis, and Z-axis noise values (in figure, dash-dot lines) are 3.40×10^{-6} (rad/s), 3.60×10^{-6} (rad/s), and 5.40×10^{-6} (rad/s), respectively. The average estimated measurement noise values (in figure, solid lines) between 15 seconds and 50 seconds are 3.50×10^{-6} (rad/s), 3.64×10^{-6} (rad/s), and 5.44×10^{-6} (rad/s). Thus, we verify that the designed adaptive Kalman filter estimates the measurement noise covariance with maximum of 2.9 percent error.

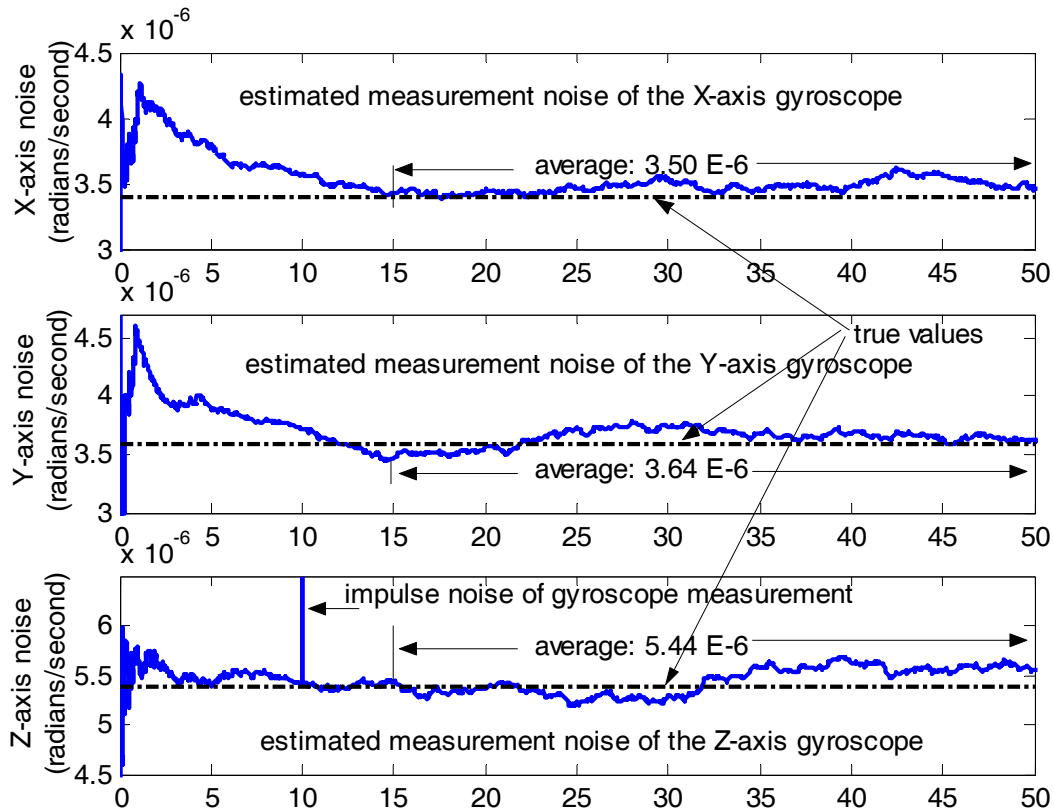


Figure 4. The estimated measurement noise covariance from the rotation vector based method.

Figure 5 shows the angle error covariance. To compare the rotation vector-based angle error covariance with the Euler angle-based error covariance, the sum of the East, North, and Up rotation vector error covariances and the sum of the roll, pitch, and yaw angle error covariances are used. The Euler angle based method reaches 0.2 degrees angle error in about 15 seconds, while the rotation vector based method reaches in about 2 seconds.

Figure 5 shows that the error covariance from the rotation vector based method is smaller by 63% than the Euler angle based method at 50 seconds. Because smaller error covariance values mean better performance, we note that the rotation vector based method is better than

the Euler angle based method. This means that the states are estimated more accurately using the rotation vectors than Euler angles.

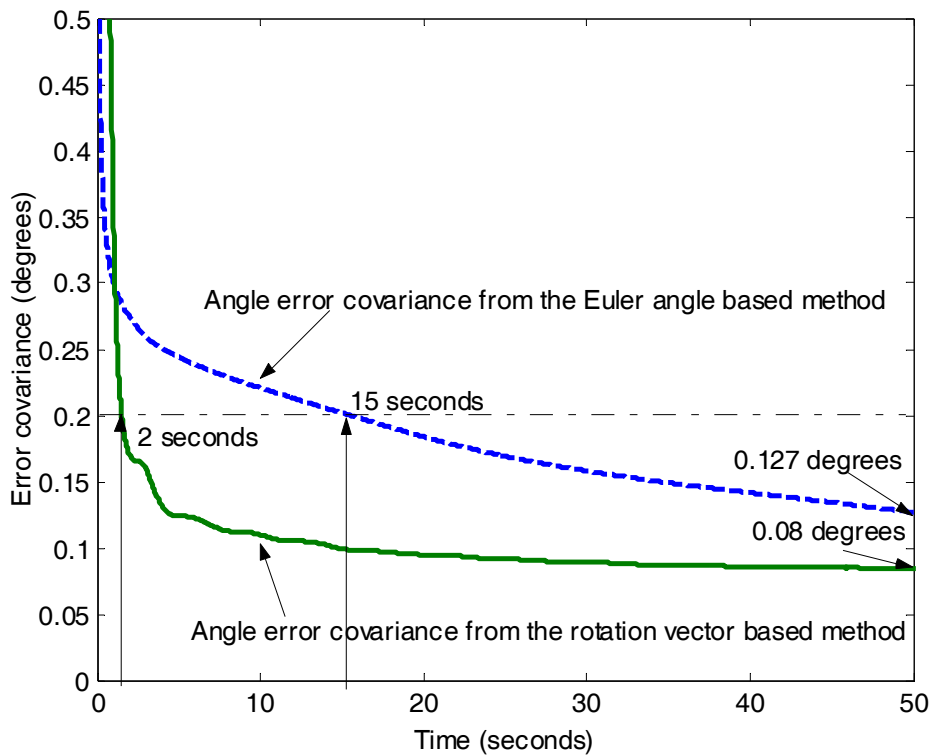


Figure 5. The angle error covariances from the simulation.

VI. Field Test

The final objective of the field test was to automatically geo-locate the aerial images. The initial alignment field test was one of the necessary steps to take before geo-locating the aerial images. The test was performed on October 1, 2003 in Grand Forks, North Dakota. Figure 6 shows the airborne cameras and IMU, which was installed on the University of North Dakota Piper airplane. For the geo-location of the airborne images, the loosely coupled DGPS/INS integration software and geo-location software were developed and used.

The overall accuracy of the DGPS/INS integration and geo-location of the airborne images depended on the initial accuracy of the IMU attitude. This initial attitude is determined from the initial fine alignment. So, the accuracy of the geo-location of the airborne images was directly related to the initial alignment accuracy.

In the initial alignment, the main difficulty was in determining the initial coarse heading angle for the IMU calibration. To get the accurate heading angle from DGPS, the vehicle X-axis and IMU X-axis was pointed in the same direction on the North-East plane of the NED coordinate frame. And the IMU was located directly below the DGPS antenna vertically. Also, to obtain accurate initial alignment, we moved the airplane in a straight line before taking off as shown in Figure 7.



Figure 6. Three airborne cameras (black boxes on the left) and an inertial measurement unit (light colored cylinder on the right).

Initially we assumed 7 degrees heading error and the vehicle moved in a straight line

for at least 10 seconds. This initial 7 degrees heading error includes the installation error, DGPS information error, and tilt angle related coupling error. As hardware equipment, the NovAtel’s OEM4 GPS receiver and Inertial Science Inc.’s tactical grade DMARS-I-N IMU were used. Table 2 shows the specification of DMARS-I-N, which includes three pendulous linear accelerometers (PLA) and two dynamically tuned gyroscopes (DTG). In Table 2, “bias” noise represents the constant bias, and “in-run bias” represents the turn-on bias, which should be compensated by the calibration procedure.

Table 2. DMARS-I-N performance specifications.

Accelerometers		Gyroscopes	
Bias (μg)	1000	Bias (Deg/hr)	5
In-run bias (μg)	< 500	In-run bias (Deg/hr)	< 1.0
Scale factor (Ppm)	300	Scale factor (Ppm)	300
Misalignment (μ -rads)	300	Misalignment (μ -rads)	300
Random noise(μg /sqrt(Hz))	50	Random noise (Deg/sqrt(hr))	0.02

Figure 7 shows pictures of the airplane when the initial heading angle determination was performed. Before the airplane took-off, the airplane followed a straight line to get the accurate heading information from the DGPS receiver. The initial heading angle from the DGPS was used as the initial azimuth angle of the IMU and airborne cameras. This was also used for the turn-on bias calibration.



Figure 7. The initial reference heading angle determination.

A. IMU Calibration

After determining the reference-heading angle, the IMU calibration was performed.

First, the Z-axis turn-on bias of accelerometer was estimated based on the coarse alignment values as

$$b_{az} = \bar{f}_z^b - g \cos(\sqrt{\phi_c^2 + \theta_c^2}), \quad (26)$$

where \bar{f}_z^b is the averaged Z-axis accelerometer output; g is the local gravity force in downward direction; and ϕ_c and θ_c are the tilt angles from the leveling test. Note that the leveling test was performed before the field test and the accuracy of the tilt angles was less than -0.06 degrees as represented in our previous work [39]. Second, the turn-on biases of the gyroscopes are estimated by assuming that the vehicle surface is placed on the true horizontal plane. By simple geometric relationships as shown in Figure 8, X-axis turn-on bias is estimated as

$$b_{gx} = \bar{\omega}_x^b - \omega_{ie} \cos(\lambda) \cos(\varphi_{DGPS}) \quad (27)$$

where $\bar{\omega}^b$ is averaged gyroscope outputs, and φ_{DGPS} is the heading information from the DGPS output. Then the turn-on bias on the gyroscope Y-axis is calculated by using the heading information as

$$b_{gy} = \bar{\omega}_y^b + \omega_{ie} \cos(\lambda) \sin(\varphi_{DGPS}), \quad (28)$$

and the turn-on bias on the gyroscope Z-axis is calculated as

$$b_{gz} = \bar{\omega}_z^b + \omega_{ie} \sin(\lambda). \quad (29)$$

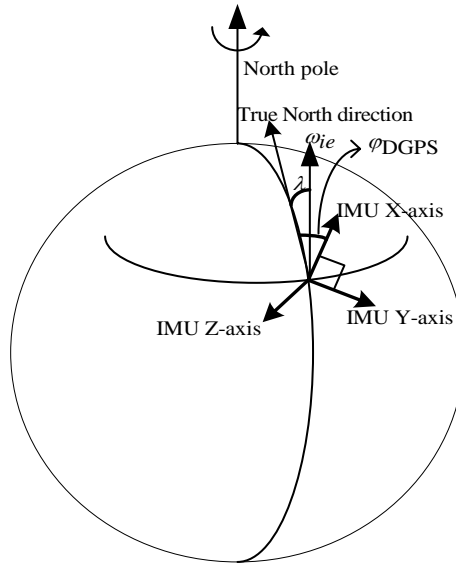


Figure 8. Geometric configuration for the gyroscope calibration.

B. Field Test Results

After compensating the calibrated bias noises, the initial alignment was performed.

Figure 9 shows the angle error covariances of the rotation vector-based alignment and Euler angle-based alignment. Figure 9 shows that 2 degrees angle error covariance was estimated

within 170 seconds from the rotation vector based method (dashed line), while 2 degrees angle error covariance was estimated within 340 seconds from the Euler angle-based method (solid line). As noted in the simulations, the field test also shows that the states are estimated more accurately using the rotation vectors than Euler angles.

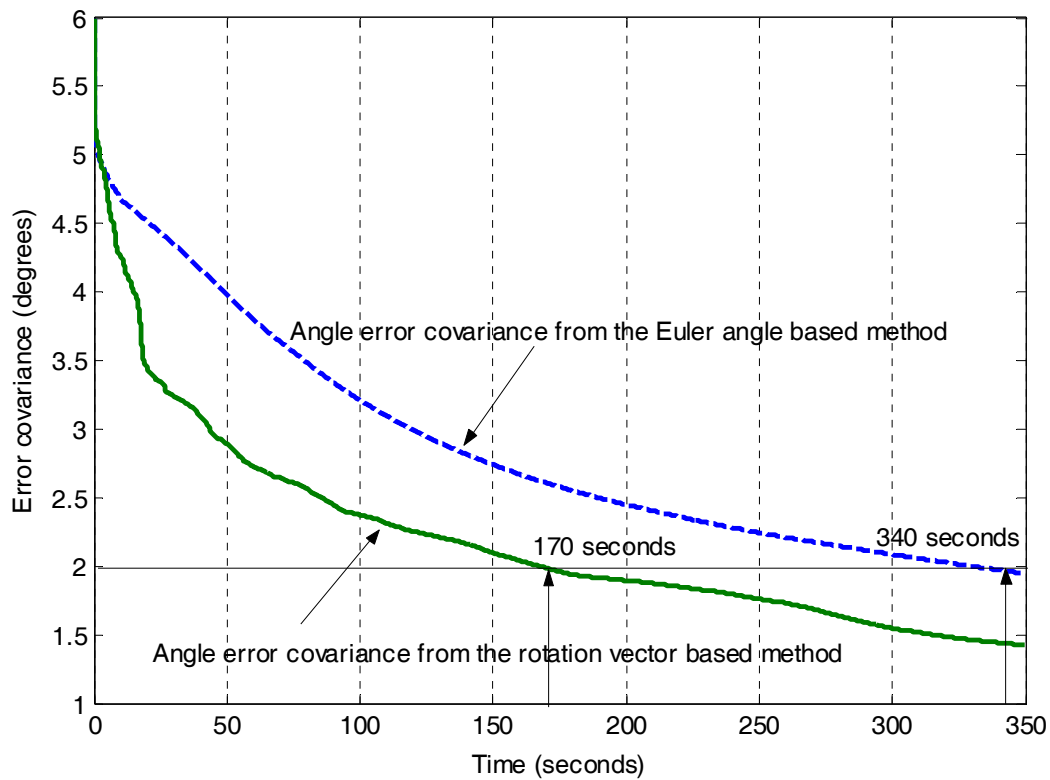


Figure 9. Estimated angle error covariance from the field test.

Figure 10 shows the estimated angle errors of two methods: Euler angle and rotation vector. The figure also shows that there is about 2.2 degrees angle error in Euler angle-based method, while there is about -1 degrees angle error in the rotation vector based method until 250 seconds. After 250 seconds, the angle error of the rotation vector method

is improved to -0.2 degrees, however, the angle error of Euler angle method did not improve.

The fast convergence characteristic of the rotation vector-based method is clearly demonstrated. We also note that there is angle error variation of 5 degrees before settling down for the rotation vector-based method, while there is 3 degrees angle error variation for the Euler angle-based method. This result shows that the large angle error was compensated quickly in the rotation vector-based method. Thus, we conclude that the rotation vector based method has much faster convergence characteristics than Euler angle based method. Faster convergence speed is directly related to shorter time necessary to perform alignment, which is an issue because the alignment must be performed before each operation and the pilots have to wait during the alignment procedure is completed. These results agree with the simulation results.

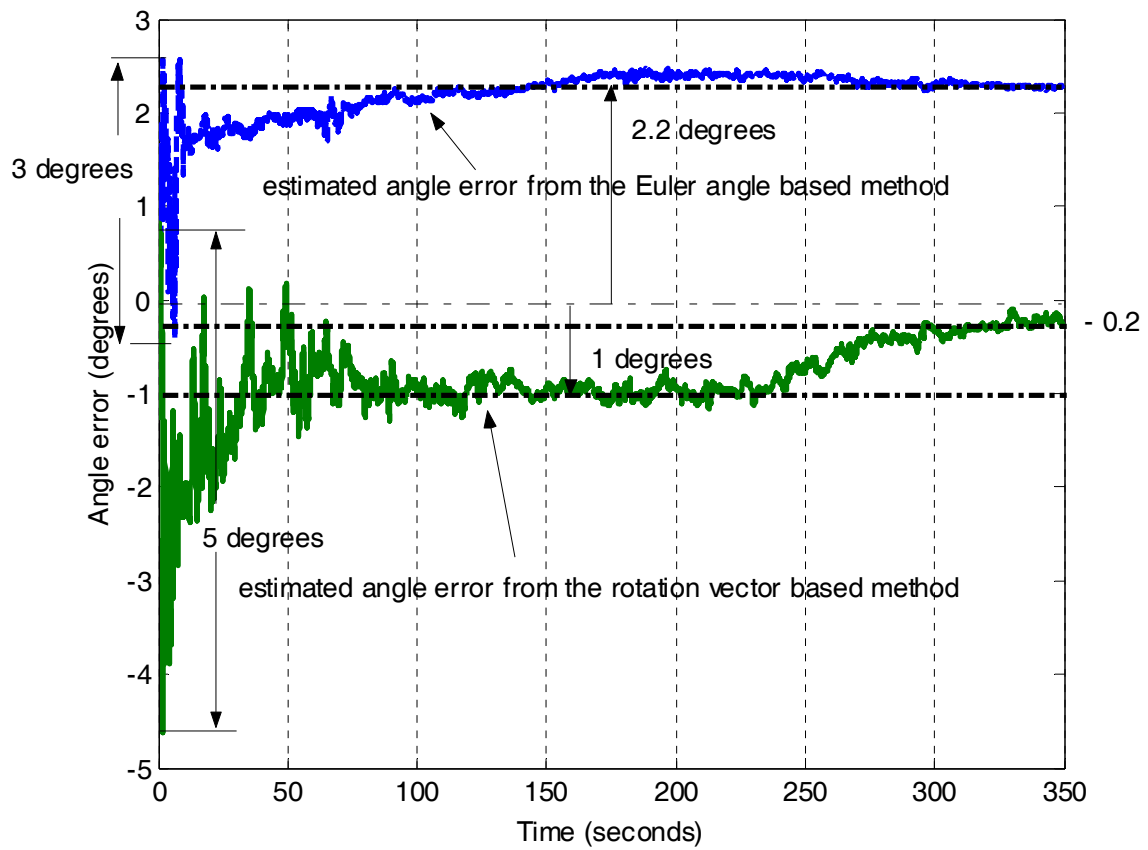


Figure 10. Angle errors from the field test.

C. Verification from the Geo-location of the Aerial Images

Finally, the geo-locations of the aerial images taken by airborne cameras were calculated using the initial attitude information of the rotation vector-based alignment.

Figure 11 shows a sample aerial image taken by the airborne camera. We assumed that the camera's line of sight direction and IMU Z-axis are pointed in the same direction. Then the position of the center of image shown in Figure 11 and the geo-located result from the geo-location software and DGPS/INS integration should be same. Note that because the DGPS/INS integration is performed on the basis of the developed initial alignment, the initial alignment accuracy is transferred to the geo-location accuracy directly. Thus, we can use the position of the center of aerial images for checking the alignment accuracy. Here, we also need reference information for the comparison. The reference position information of the center of image was calculated by a commercial software package called digital orthophoto quadrangle (DOQ). From the comparison of the geo-located center of image position with the center position calculated using DOQ, we found that there are 70 meters difference in latitude and 98 meters difference in longitude. These errors are not absolute errors, but they are relative errors with respect to a commercial software package DOQ. These errors are due to line-of-sight misalignment, GPS receiver, the Earth model, time synchronization, etc. Note that without ground fine alignment, but only with coarse alignment, we had 400 meters to 600 meters difference in both latitude and longitude. So, it

is clear that the fine alignment improved the accuracy of the geo-locations of the aerial images. Also these errors seem large compared to some commercially available package such as Applanix Corporation's POS/AV (Position and Orientation System for Airborne Vehicles) which gives a single digit accuracy for position, however, they use higher grade IMU and the alignment error between the camera and the INS is not included.

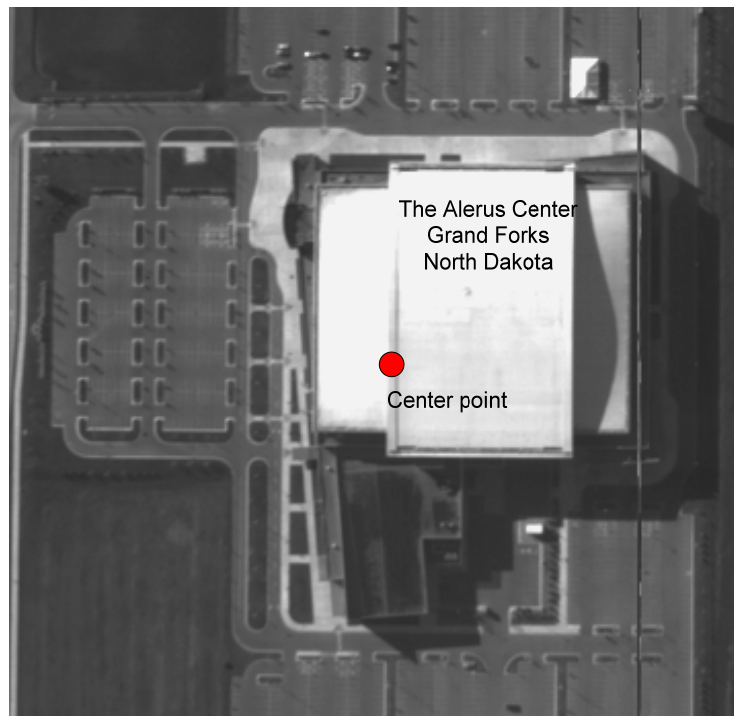


Figure 11. An aerial image taken by an airborne camera.

VII. Conclusions

In this paper, we compared the rotation vector-based alignment method with the existing Euler angle-based alignment method. From the simulations and a field test, we

found out that the rotation vector-based method has faster convergence characteristics than Euler angle-based method. Moreover, in this paper, the adaptive Kalman filter was used for the automatic measurement noise covariance determination. From the simulation test, we verified the designed adaptive filter estimates the true noise covariance values with less than 2.9 percent error. Faster convergence characteristics and automatic tuning capability give us the operational convenience of the alignment software in addition to the short alignment time. Furthermore, we checked the alignment accuracy using airborne images. By comparing the calculated center of aerial images with the calculated position using a commercial software package, DOQ, we verified that the DGPS/INS integration using the rotation vector based alignment method provides relative error of much less than 100 meters. In summary, from the fact that the simulation results are satisfactory and the field test results are acceptable for our aerial imaging system, we conclude that the rotation vector improves the convergence speed in alignment process, and the adaptive Kalman filter allows automatic measurement noise covariance tuning capability.

Acknowledgements

This research was supported in part by NASA Grant NAG13-01006, NAG13-02047, and NSF grant ECS-0428546. Authors thank the AEROCam team; Douglas Olsen, Bjorn Dahlen, Robert Nelson, Paul Virden, Richard Schultz, Arnold Johnson, William Semke, and George Seielstad for their support throughout the project.

References

- [1] Robert M. Rogers, *Applied Mathematics in Integrated Navigation Systems*, AIAA, 2000.
- [2] Robert M. Rogers, 'IMU In-Motion Alignment without Benefit of Attitude Initialization', *ION 1997 National Technical Meeting –“Navigation and Positioning in the Information Age,”* January 14-16, 1997.
- [3] Robert M. Rogers, "Low Dynamic IMU Alignment," *IEEE Position Location and Navigation Symposium*, 1998.
- [4] Oleg Salychev, *Inertial Systems in Navigation and Geophysics*, Bauman MSTU Press, Moscow, 1998.
- [5] Jay A. Farrell, and Matthew Barth, *The Global Positioning System & Inertial Navigation*, McGraw-Hill, 1998.
- [6] Mohinder S. Grewal, Angus P. Andrews, *Kalman Filtering Theory and Practice*, Prentice Hall, 1993.
- [7] P. Picard, J. F. Lafay, "Weak observability and observers for linear neutral delay-differential systems," *European Control Conference 1997*, Brussels, July 1-4, 1997.
- [8] Eduardo Nebot, Hugh Durrant-Whyte, "Initial calibration and alignment of Low cost Inertial Navigation Units for land vehicle applications," *Journal of Robotics System*, Vol. 16, No. 2, 1999, pp. 81-92.
- [9] J. Aranda, J. M. De La Cruz, S. Dormido, P. Ruiperez, R. Hernandez, "Reduced-order Kalman Filter for Alignment," *Cybernetics and Systems: An International Journal*, Vol. 25, 1994, pp. 1-16.
- [10] Robert Grover Brown, Patrick Y.C. Hwang, *Introduction to Random Signals and Applied Kalman Filter*, John Wiley & Sons, 1997.
- [11] Jiang Cheng Fang, De Jun Wan, "A Fast Initial Alignment Method for Strapdown Inertial Navigation System on Stationary Base," *IEEE Transactions on Aerospace and Electronic Systems*, Vol. 32, No. 4, 1996.
- [12] John Baziw, Cornelius T. Leondes, "In-Flight Alignment and Calibration of Inertial Measurement Units-Part I: General Formulation," *IEEE Transactions on Aerospace and Electronic Systems*, Vol. AES-8, No. 4, 1972.
- [13] John Baziw, Cornelius T. Leondes, "In-Flight Alignment and Calibration of Inertial Measurement Units-Part II: Experimental Results," *IEEE Transactions on Aerospace and Electronic Systems*, Vol. AES-8, No. 4, 1972.
- [14] Mohinder S. Grewal, Vinson D. Henderson, Randy S. Miyasako, "Application of Kalman Filtering to the Calibration and Alignment of Inertial Navigation System," *IEEE Transaction on Automatic Control*, Vol. 34, No. 1, 1991.
- [15] Sherryl H. Stovall, *Transfer Alignment*, Naval Air Warfare Center Weapons Division, China Lake, CA, 1996.
- [16] Anthony Lawrence, *Modern Inertial Technology*, Springer, 1998.

- [17] Kenneth R. Britting, *Inertial Navigation System Analysis*, Wiley Interscience, 1971.
- [18] Mohinder S. Grewal, Lawrence R. Weill, and Angus P. Andrews, *Global Positioning systems, Inertial Navigation and Integration*, Wiley Interscience, 2001.
- [19] Bortz, J. E., "A new mathematical formulation for strapdown inertial navigation," *IEEE Transactions on Aerospace and Electronic Systems*, Vol. AES-7, No. 1, 1971.
- [20] Ignagni, M. B., "On the orientation vector differential equation in strapdown inertial systems," *IEEE Transactions on Aerospace and Electronic Systems*, Vol. 30, No. 4, 1994.
- [21] Jiang, Y. F., Lin, Y. P., "On the rotation vector differential equation," *IEEE Transactions on Aerospace and Electronic Systems*, Vol. 27, No. 1, 1991.
- [22] Malcolm D. Shuster, "The kinematic equation for the rotation vector," *IEEE Transactions on Aerospace and Electronic Systems*, Vol. 29, No. 1, 1993.
- [23] George M. Siouris, *Aerospace Avionics Systems*, Academic Press, Inc. 1993.
- [24] D. T. Magill, "Optimal adaptive estimation of sampled stochastic processes," *IEEE Transaction on Automatic Control*, Vol AC-10, No. 4, 1965, pp. 434-439.
- [25] Peter K. S. Tam, John. B. Moore, "Adaptive estimation using parallel processing," *Technical Report EE7411*, Department of Electrical Engineering, University of Newcastle, 1974.
- [26] David W. Kyger and Peter S. Maybeck, "Reducing lag in virtual displays using multiple model adaptive estimation," *IEEE Transactions on Aerospace and Electronic Systems*, Vol. 34, No. 4, 1998.
- [27] Peter D. Hanlon and Peter S. Maybeck, "Interrelationship of single-filter and multiple-model adaptive algorithms," *IEEE Transactions on Aerospace and Electronic Systems*, Vol. 34, No. 3, 1998.
- [28] Antal Soos, and O. P. Malik, "AUPEC2002 - An optimal Adaptive Power System Stabilizer," *Australasian Universities Power Engineering Conference*, Melbourne, Australia, 29 September - 2 October 2002.
- [29] Robert D. Turney, Ali M. Reza, and Justin G. R. Delva, "FPGA Implementation of Adaptive Temporal Kalman Filter for Real Time Video Filtering," *1999 IEEE International Conference on ACOUSTICS, SPEECH, AND SIGNAL PROCESSING*, Phoenix, Arizona, 15-19 March, 1999.
- [30] Jinling Wang, Chris Rizos, Mike P. Stewart, and Alfred Leick, "GPS and GLONASS Integration: Modeling and Ambiguity Resolution Issues," *GPS Solutions*, 5(1), 2001, pp. 55-64.
- [31] Dai, Liwen, "Dual-Frequency GPS/GLONASS Real-Time Ambiguity Resolution for Medium-Range Kinematic Positioning," *13th Int. Tech. Meeting of the Satellite Division of the U.S/ Inst. Of Navigation*, Salt Lake City, Utah, 19-22 September, 2000, pp. 1071-1080.

- [32] P. Wira, J. P. Urban, "A New Adaptive Kalman Filter Applied to Visual Servoing Tasks," *Proc. of 4th International Conference on Knowledge-Based Intelligent Engineering Systems & Allied Technologies*, Brington, UK, 2000.
- [33] P. Wira, J. P. Urban, and J. Cresser, "A Divide and Conquer Learning Architecture for Predicting Unknown Motion," *ESANN 2001 proceedings - European Symposium on Artificial Neural Networks*, Bruges, Belgium, 25-27 April 2001.
- [34] B. D. Dakshayani, M. R. Ananthasayanam, and N. V. Vighnesam, "Adaptive Kalman Filtering Technique for Relative Orbit Estimation for Colocated Geostationary Satellite," *Satellite Performance Workshop*, Laurel, Maryland, 18-19 September 2001.
- [35] R. M. O. Gemson, M. R. Ananthasayanam, and M. R. Muralidharan, "A Graphical User Interface for an Adaptive Extended Kalman Filter Program for Aircraft Parameter Estimation Studies," *Proceedings of the Meeting of the Japan Society for Aeronautical and Space Sciences (JSASS)*, Sendai, Japan, October 11-13, 2000.
- [36] Nicolas Obolensky, Deniz Erdogmus, Jose C. Principe, "An Time-Varying Kalman Filter Applied to Moving Target Tracking," *Proceedings of CONTROLO'02*, Aveiro, Portugal, September 2002, pp. 418-422.
- [37] Sasiadek J. Z, Q. Wang, "Sensor Fusion Based on Fuzzy Kalman Filtering for Autonomous Robot Vehicle," *Proc. 1999 IEEE International Conference on Robotics and Automation*, 1999, pp. 2970-2975.
- [38] Peter S. Maybeck, *Stochastic Models, Estimation, and Control Volume 2*, Navtech Book and Software Store, 1994.
- [39] Hyo-Sung Ahn, Chang-Hee Won, Douglas Olsen, Richard R Schultz, Arnold Johnson, William Semke, George Seielstad, and Chuck Wivell, "Attitude Estimation of the Tactical Grade Inertial Measurement Unit for Airborne Environmental Camera," *Proceeding of American Control Conference*, Denver, June 4-6, 2003, pp. 4403-4408.